JLAB12 Activity report 2021

M. Mirazita (Resp.), D. Orecchini(Tecn.), P. Rossi, O. Soto (INFN fellowship), S. Tomassini

1 Introduction

The JLAB12 group of LNF participates in the physics program carried on by the CLAS collaboration in the Hall B of the Jefferson Laboratory (JLab). Most of the work of the LNF group this year was dedicated to the study of the performance of the first RICH module with physics data. In parallel, the construction of the second RICH module is underway.

2 The CLAS12 RICH

The detector is composed by an aerogel radiator, an array of multianode photomultiplier tubes (MAPMTs) for the Cherenkov light detection and a mirror system. All these elements are contained in a large trapezoidal box, of approximate height of 3.5 m and large base of about 4 m.

The radiator is composed by tiles with squared shape 20×20 cm^2 as well as smaller pentagonal, trapezoidal or triangular tiles to accomodate with the detector shape. The total number of tiles is 102, assembled in two sections: the forward angle one made by one layer with 2 cm thickness and the large angle one made by two layers with 3 cm thickness each.

The mirror system is composed by 10 carbon fiber spherical mirrors and 7 glass planar mirros, for a total surface of about 10 m^2. The goal of the mirror system is to contain as much of the produced Cherenkov photons inside the detector and to direct them toward the photodetector array.

The photodector array uses 391 MAPMT Hamamatsu H8500 and H12700. These two types of tubes are composed by a matrix of 8×8 matrix of pixel with about 6 mm pixel size, with a total of 25024 independent readout channels.

The readout electronics is based on the MAROC3 chip, a 64 channel microcircuit dedicated to MAPMT pulse processing. Each channel offers a low impedence adjustable gain preamplifier followed by a highly configurable shaping section, and produces prompt logic pulses from an adjustable threshold discriminator. The MAROC is configured and read out by a FPGA optically linked with the data acquisition node. The front-end electronics is organized in compact units mechanically designed to fit the MAPMT dimensions and serving two or three MAPMTs each, thus allowing the tessellation of large surfaces with minimum dead space and material budget.

3 Reconstruction of the RICH data and particle ID performance

The first RICH module, installed in 2017, has been successfully together with the rest of the CLAS12 during all the data taking periods completed so far. The physics data collected have been used to carefully review the performance of the detector.

The reconstruction of the RICH data follows a number of successive steps. The first step is the translation, for each readout channel, of the electronics address into a physical address, composed

by the photomultiplier ID and the anode number. A first selection of the recorded hit is then done, to separate clusters of hits, produced by the charged particles hitting the entrance window of the MaPMT, from single hits. The single hits are further classified in photon hit candidates, passed to the following reconstruction steps, and cross-talk hits, that are not analyzed further.

Photon hit candidates are processed through a ray tracing algorithm. The starting point of the algorithm is the photon production vertex, determined by projecting the charged tracks to the aerogel surface. Then, the algorithm traces photon paths from the production vertex to the PMT hit position through the various optical elements of the RICH (aerogel radiator, mirrors, MAPMT photocathode). By minimizing the distance between the real and traced hit position, the Cherenkov emission angle corresponding to each hit can be computed. When more than one track crossed the RICH, each detected hit will be associated to one possible Cherenkov angle value per track.

Once the Cherenkov angles have been reconstructed, a likelihood-based approach has been implemented in order to perform the final particle identification [1)]. For each possible particle species, a probability is calculated, based on the likelihood that the observed photons are compatible with the expected Cherenkov angle, given the refractive index of the tile crossed by the charged track and the momentum of the track. Four possible particle species are considered (electrons, pions, kaons, protons) although electrons are not taken into account in the final ID. At the end, at each track the particle ID with highest probability is attributed, with a quality parameter defined by

$$Q = 1 - \frac{P_2}{P_1} \tag{1}$$

where P_1 and P_2 are the best and second best probabilities, respectively.

3.1 Alignment of the detector

An important part of the calibration process is the precise aligment of the RICH detector. The first step is the alignment of the whole detector to the rest of the CLAS12, obtained by comparing the position of the charged particle clusters produced on the MAPMTs and the projection of the recontsructed tracks in CLAS12 to the RICH MAPMT plane.

Then, all the other optical elements (mirrors and radiators) of the RICH must be alignned with respect to the MAPMT plane. For each element, a set of three rotation angles and three position offsets can be defined. In order to minimize the number of free parameters, in first approximation one angle and two offset can be neglected, ending up with three free parameters per each element: 3 aerogel planes, 7 planar mirrors and 10 spherical mirrors.

The aerogel radiator position is determined by selecting β =1 particles (particles identified in CLAS12 either as electrons or pions with momentum above 2 GeV/c) and photons that are reconstructed without reflections on the mirrors (direct photons) and minimizing the difference between the measured Cherenkov angle and the one obtained from the refractive index value measured during the characterization of the aerogel tiles. Then, the alignment parameters of the mirrors are determined by imposing that the Cherenkov angle of the photons reconstructed after one or more reflection is the same of the direct photons.

In the Fig. 1 we show some plot obtained using tracks passing through the aerogel tile 5 of the lower angle sector of aerogel with 2 cm thickness. The top left plot shows the Cherenkov angle measured for electron tracks using direct photons (blue histogram) and photons with one reflection on the planar mirror A1L. The peak position shows several mrad of difference. After the alignment, the two peaks almost concide (top right plot). The quality of the alignment is further demostrated by comparing the measured Cherenkov angle for electrons with those for pions (bottom left plot) or the Cherenkov angle for electrons with two opposite polarities of the torus field (bottom right).

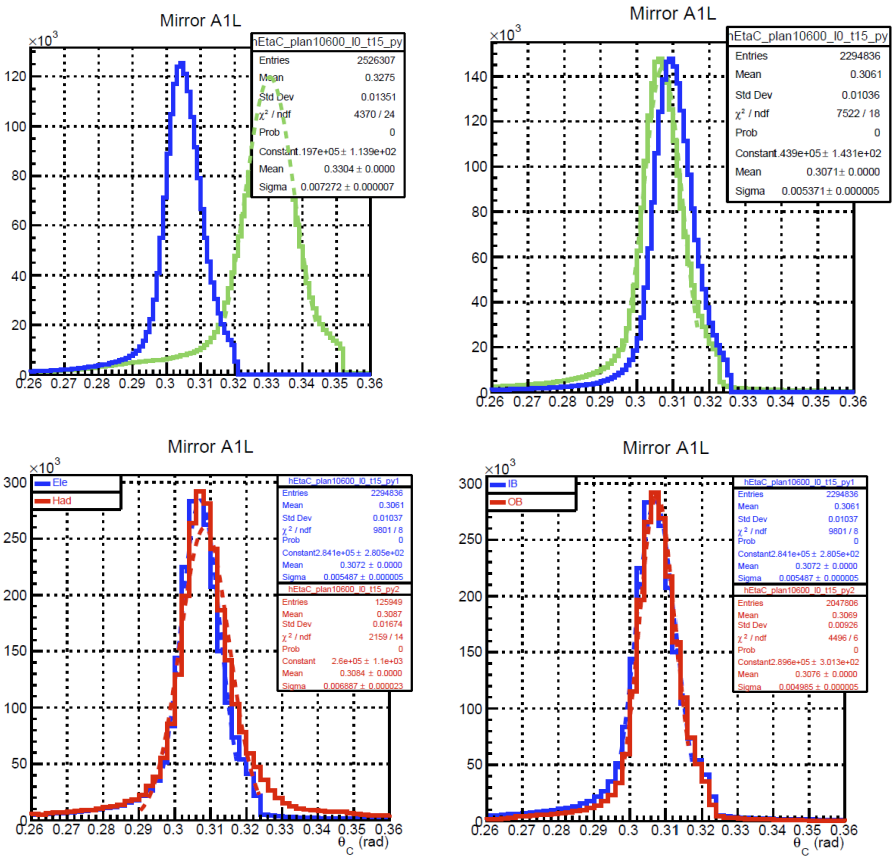

Figure 1: *Alignment of the planar mirror A1L, Cherenkov angle for tile 15 of aerogel layer 0. Top row: comparison between the direct (in blue) and reflected (in green) photons before (left) and after (right) the alignment of the mirror. Bottom row, left: comparison between the reflected photons from electrons (blue) and pions (red). Bottom right: comparison between the reflected photons for electrons with two opposite torus field.*

The alignment procedure considered separately each element using the simplest photon detection configuration. This procedure worked reasonably well in simple cases, as shown in Fig. 1, but failed to provide acceptable results for more complicated configuration, for example the ones with more than one reflection. This is shown in Fig. 2, where we compare the Cherenkov angle of direct photons (in blue) with the one for photons with first reflection on the spherical mirror 1 (in pink). The double peak in the latter is most likely due to the contribution of several different detection topologies. For example, after the first reflection the photon can be directed toward the MAPMTs with a second reflection on one of the two frontal mirrors B1 or B2.

It is clear that the simplified alignment procedure used so far cannot properly take into account all the correlations between the various photon detection topologies. For this reason, a project aimed at performing the alignment using a machine learning approach has started.

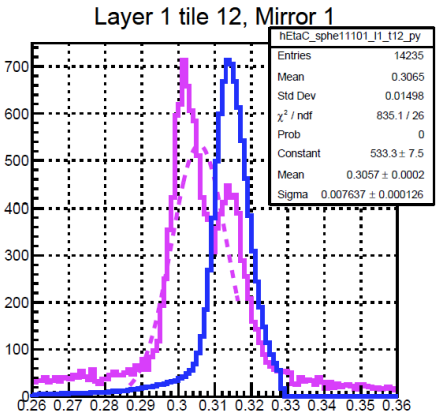

Figure 2: *Alignment of the planar spherical mirror 1, Cherenkov angle for tile 1 of aerogel layer 1: the blue histograms is for direct photons, the pink one for photons with first reflection on the spherical mirror.*

3.2 Calibration of the detector

In order to obtain a reliable PID information, a precise knowledge of the refractive index of each aerogel and of the single photon angular resolution is mandatory. This is achieved selecting $\beta = 1$ particles and plotting the reconstructed Cherenkov angles. Because of the complicated optics of the RICH, and given the fact that slightly misalignements of the mirrrors can produce a non negligible shitf in the measured Cherenkov angle, as was discussed in the previous section, calibration tables of the refrctive index per tile are produced for three different sets of photons:

- direct photons, i.e. photons detected without any reflection;
- photons with first reflection on a lateral mirror;
- photons with first reflection on a spherical mirror.

Mean and gaussian widths of these distribution are stored in the CLAS database.

3.2.1 Particle identification with the RICH

The likelihood approach in the RICH particle identification requires a good knowledge of the expected Cherenkov angle for all the possible hadron species, all the aerogel tiles and all the photon detection configurations. This has not been achieved so far for the configuration involving the spherical mirrors, as discussed in the previous sections. For this reason, the RICH PID has been restricted to photons detected either directly or after reflections on the planar mirrors only. This requirements restricted the kinematic plane covered by the RICH to the most forward angles only, up to about 15^o for inbending particles and about 20^o for outbending particles.

An effective way to monitor the goodness of the particle identification is to at look mass distributions involving kaon. We will consider here the missing mass of the reaction $ep \to e'K^+X$. The scattered electron is detected in CLAS12 in all sectors except for sector 4, where the RICH is installed, while the kaon candidate is detected in sector 4. In the Fig. 3, we show this missing mass distribution with kaons identified in CLAS12 without the RICH. On top of a broad continuum distribution, the plot also shows a prominent peak at $MM \approx 1.15$ GeV corresponding to reactions

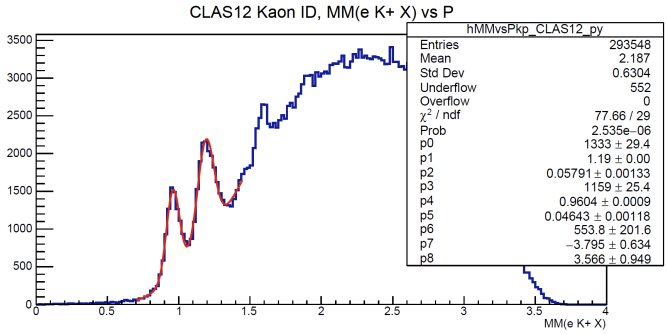

Figure 3: *Missing mass of the* $ep \to e'K^+X$ *reaction with the scattered electron and the kaon identified in CLAS12 without the RICH.*

with missing Λ or Σ^0 and a smaller peak corresponding to the $\Lambda(1520)$. It also shows a prominent peak in the nucleon mass region. This peak is clearly a fake due to pions misidentified as kaons from the exclusive reaction $ep \to e'\pi^+(n)$.

The same missing mass is ahown in Fig. 4, in which the kaon identification is performed using the RICH. We see several features comparing this plot with the Fig. 3:

- an overall reduction in the total number of events, partly due to the limited kinematic coverage of the RICH in the present analysis and partly due to the suppression of the pion misidentification;
- an increas in the signal-to-background ratio in the region of the Λ or Σ^0;
- the fake nucleon peak almost disapperead;

The almost disappearance of the fake nucleon peak and the increased S/B ratio in the Λ or Σ^0 region are clearly signaling the improvement in the kaon ID with the RICH. On the other hand, the small residual nucleon peak is an indication of the need for further improvements in the RICH ID. This residual misidentified pions comes mainly from the edges of the kinemaitcs: larger angles where the number of photons is small or higher momenta where the π/K separation is more difficult.

The inclusion of the photons reflected by the spherical mirrors not only will extend the kinematic coverage, but also will improve the π/K rejection power by adding more photons in the likelihood calculation. We also expect better PID results from the alignment process based on the machine learning that is currently underway.

3.2.2 RICH software

A considerably effort was dedicated to the development and testing of the software to handle the RICH data. This included the calibration suites to extract all the relevant parameters for the particle ID algorithm, testing the results of the Cherenkov angle reconstruction in the various photon detection configuration, optimization of the likelihood algorithm, etc.

In 2021 we also started a detailed revision of the available software to be able to include the second RICH module as soon as it will be installed and turned on.

4 Construction of the second RICH module

The contruction of the second RICH module, with the same geometry of the first one, is currently underway under the supervision of the physicists, technologits and technicians of the LNF group.

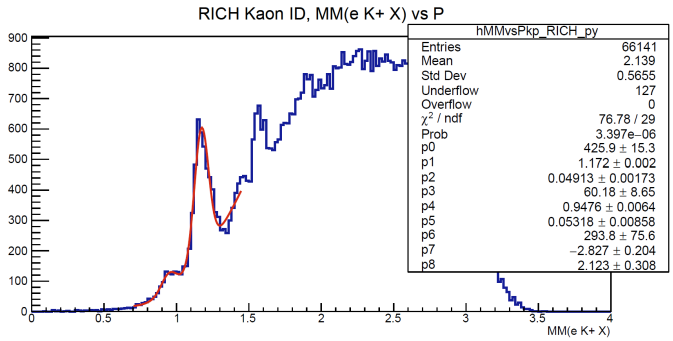

Figure 4: *Missing mass of the* $ep \rightarrow e'K^+X$ *reaction with the scattered electron identified in CLAS12 and the kaon in the RICH.*

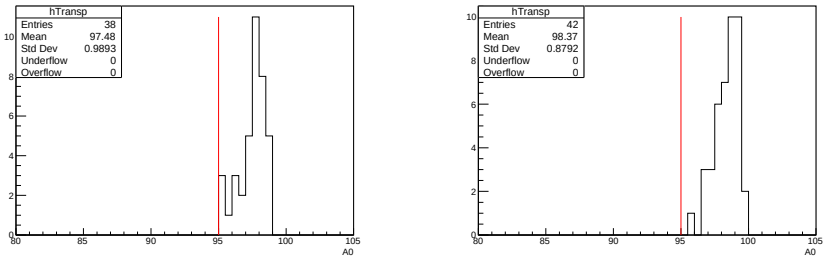

Figure 5: *Transparency parameter for the 38 tiles installed in the first module (left plot) and for the 42 tiles available for the second module (right plot).*

The production of all the components is almost completed, with all of them already shipped to Jefferson Lab. The plan is to start the assembly work in January 2022, with the goal to have the module completed and installed in the CLAS12 by the end of May 2022, ready for the beginning of the data taking with longitudinally polarized hydrogen target planned in the first week of June 2022.

4.1 The mechanical structure

The mechanical structure has been shipped to Jefferson Lab in the first months of 2021.

4.2 The aerogel radiator

In 2021 the production of the aerogel radiator has been completed with the last lateral tile of the section with two layer of tiles of 3 cm thickness. All the tiles have been shipped to the Jefferson Lab. The characterization parameters of the tiles showed a slight increase in the optical performance with respect to the aerogel of the first module. As an example, in Fig. 5 we show the transparency parameter A_0 for the 38 tiles with 2 cm thickness installed in the first module (on the left) and the same parameter for the 42 tailes available for the second module (right plot), including the four lower quality spares from the first module.

4.3 The planar mirrors

The production of the planar mirrors has been completed in 2021 and all the mirrors have been already shipped to the Jefferson Lab.

4.4 The spherical mirrors

The spherical mirrors have been produced during 2021 by the same company that produced the mirrors for the first module. The mirrors have been produced using a new glass mold that has been also purchased in 2021, because the one used in the past was not available any more. The carbon fiber frame to install the mirrors in the RICH is in production by the same company. The design of this frame has been revised upon request by the company to simplify the production process and reduce the costs. In particular, the stright sections of the old design have been replaced by curved ones, with the same radius of curvature of the mirrors. Besides the easier assembly of the frame, this new design should also provide a better performance, because all the mounts fixing the single mirrors to the frame have now the same length.

Two mirrors have been delivered to the Jefferson Lab for inspection and characterization tests. The main characterization test was the so-called D_0 test, which is the measurement of the size of the reflected spot when the mirror is illuminated by a point-like light source positioned at the center of curvature of the mirror. The D_0 is connected to the angular resolution σ_θ by the equation

$$\sigma\theta = \frac{D_0}{8R} \tag{2}$$

where R is the radius of curvature. The specification for the mirrors, a D_0 smaller than 2.5 mm corresponding to an angular resolution of 0.1 mmrad, is really stringent and ensure basically a negligible contribution to the total angular resolution of the Cherenkov photons in the RICH. In Fig. 6, we show the measured spot size measured for the mirror 5 central as a function of the position of the stepper motor that is moving longitudinally the light source and the photocamera. At minimum, the spot has $D_0 = 2.1$ mm, still within the specifications but a bit worse than the mirrors of the first module. A similar result was obtained for the mirror 2 also tested at Jefferson Lab. This was attributed part to the new mold and part to a new core structure, that might induce slight astigmatism in the mirror surface. A systematic program of measurement on all the mirrors is planned for the beginning of 2022, before sending the mirrors to the company that will perform the deposition of the reflecting layer.

4.5 The photomultipliers

The production of 400 Hamamatsu H12700 Multi-Anode PMT has been completed in 2021. All the tubes have been tested to verify the agreement with the specifications and to characterize the repsonse in the single photon regime. For these tests, the same electronics used on the RICH readout has been used. The tests included measurements of the single photon spectrum with both scaler and ADC readout and the measurement of the dark count rate. Only few pieces were found not within the specifications and promptly replaced by the company.

As an example of the results of the test, we show in Fig. 7 the dark count rate measured for all the anodes of the 400 MAPMTs at the standard operating HV for the RICH of 1000V (left plot) and at 1100 V (right plot), the maximum recommended by Hamamatsu. The specification limit was 2.5 kHz on average on the whole MAPMTs at 1000V. All the MAPMTs are within the specification and only a very small fraction of single pixels (of the order of ten out of more than 25000) exceeded this limit.

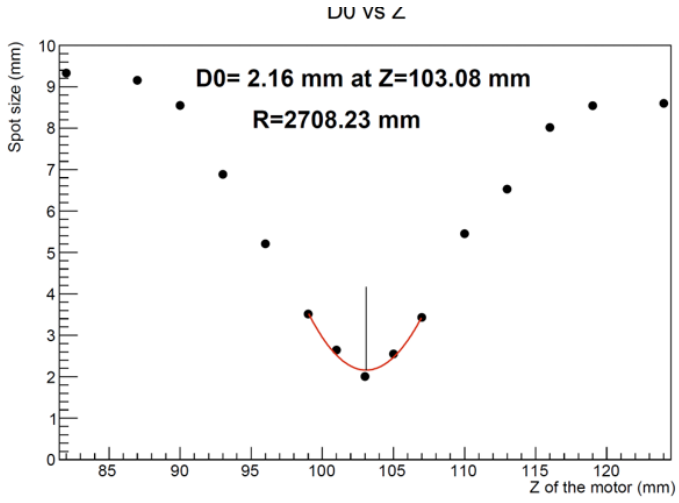

Figure 6: *The D_0 curve measured on the mirror 5 central.*

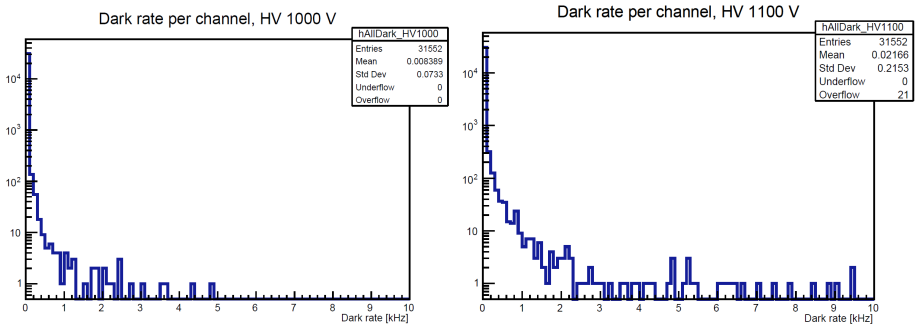

Figure 7: *The dark count rate per pixel measured on the 400 MAPMTs at 1000V (left) and 1100V (right). Note that some of the MAPMT has been tested more than once.*

4.6 The front end electronics

The front end electronics is organized in units composed by an adapter board, a MAROC board hosting the chip for the readout of the MAPMT and a FPGA board in charge of configuring the MAROC chips and connecting the RICH readout to the CLAS12 DAQ. The production of the adapter and MAROC board is in charge to the INFN, while the production of the FPGA boards is in charge of the Jefferson Lab.

All the adapter boards have been produced and shipped to the Jefferson Lab. During the production of the MAROC boards, some issues were encountered due to the lower quality of some of the chips purchased (at lower price) in 2020 by the Omega producer [2]. For this reason, a new batch of chips, at a price increased by a factor 3, have been purchased from CAEN and new MAROC boards are in production. The production of the FPGA boards also started in the last months of 2021. We plan to have all the front end boards available at Jefferson Lab by the first months of 2022.

4.7 The services

The services are in charge of the Jefferson Lab. They include

- the nitrogen system to purge the RICH detector and keep the internal humidity at few percent level;
- the front end electronics cooling system;
- the low and high voltage power supply;
- the electronics for the data acquisition;
- the slow controls to handle and monitor the high and low voltages and to monitor the performance of the detector;

The production of all these systems, that will replicate the ones of the first module, is in progress. All of them will be extensively tested during the assembly of the detector and also during the commissioning of the detector after its installation in CLAS12.

References

1. A. Schoning, LHC-B/97-018 (1997).
2. Omega website: http://omega.in2p3.fr